Structure and dynamics of the insulin receptor: implications for receptor activation and drug discovery

Libin Ye[1], Suvrajit Maji[1], Narinder Sanghera[2], Piraveen Gopalasingam[2], Evgeniy Gorbunov[3], Sergey Tarasov[3], Oleg Epstein[4] and Judith Klein-Seetharaman[1,2]

[1] Department of Structural Biology, University of Pittsburgh, Pittsburgh, PA 15260, USA
[2] Division of Metabolic and Vascular Health & Systems, Medical School, University of Warwick, Coventry CV4 7AL, UK
[3] OOO 'NPF 'MATERIA MEDICA HOLDING', 47-1, Trifonovskaya St, Moscow 129272, Russian Federation
[4] The Institute of General Pathology and Pathophysiology, 8, Baltiyskaya St, 125315 Moscow, Russian Federation

Recently, major progress has been made in uncovering the mechanisms of how insulin engages its receptor and modulates downstream signal transduction. Here, we present in detail the current structural knowledge surrounding the individual components of the complex, binding sites, and dynamics during the activation process. A novel kinase triggering mechanism, the 'bow-arrow model', is proposed based on current knowledge and computational simulations of this system, in which insulin, after its initial interaction with binding site 1, engages with site 2 between the fibronectin type III (FnIII)-1 and -2 domains, which changes the conformation of FnIII-3 and eventually translates into structural changes across the membrane. This model provides a new perspective on the process of insulin binding to its receptor and, thus, could lead to future novel drug discovery efforts.

Introduction

The insulin receptor (IR) has a pivotal role in the regulation of glucose homeostasis, and its dysfunction can result in a range of clinical manifestations, including diabetes mellitus and cancer. The cDNA of IR was cloned and sequenced during the 1980s [1], and gives rise to a protein with subunit composition α2β2 [2] (Fig. 1a) with a molecular weight of approximately 350 kDa [3]. The α-subunits are located on the extracellular (EC) side of the plasma membrane, and are similar in domain organization to the Epidermal Growth Factor receptor ectodomain [4] and the insulin-like growth factor 1 receptor [5]. Despite these general similarities, there are also important differences [6,7]; therefore, here we focus on IR for brevity and clarity. In addition to the ectodomain, IR also contains a transmembrane (TM), juxtamembrane (JM), and cytoplasmic (CP) tyrosine kinase (TK) domain within its β-subunit. Activation of the TK constitutes the hallmark of receptor signaling upon insulin binding [8]. The first crystal structure of the basal (inactive) TK was reported in 1994 [9]. Eleven inactivated and activated TK structures have since been documented (Fig. 1c). The structure of the IR ectodomain dimer was first reported in 2006 and a higher resolution structure of insulin engaging binding site 1 was reported in 2013 [10], which was further improved recently [11]. There is no full-length IR structure so far because of the high flexibility of the intact IR and its membrane-bound nature [12]. Here, we summarize the structure, conformation, and dynamics of IR to gain insight into receptor activation, which is indispensable for understanding receptor function, such as the mechanisms of naturally occurring mutations causing disease, allostery, and negative cooperativity, differences between the two IR-A and IR-B isoforms and, related to these, deciphering mitogenic versus metabolic effects of receptor signaling. A better understanding of the links between structure, dynamics, and function could infuse drug development efforts.

Corresponding author: Klein-Seetharaman, J. (J.Klein-Seetharaman@warwick.ac.uk)

http://dx.doi.org/10.1016/j.drudis.2017.04.011

The structures of the individual components

Structure and dynamics of the IR ectodomain

Each insulin ectodomain monomer includes the whole α-chain and 194 residues of each β-chain, comprising two leucine-rich repeat domains (L1-L2), a cysteine-rich region (CR), and three fibronectin type-III domains (FnIII-1–3) [13,14]. FnIII-2 is the site of cleavage into α- and β-chains, which splits this domain into five segments: FnIII-2a, insert domain (ID-α, residues 639–692), and C-terminal domain (αCT, residues 693–719) at the end of the α chain, and ID-β (residues 724–754) and FnIII-2b at the beginning of the β chain [6]. In IR-B (also referred to as 'isoform long'), there is a 12-amino acid insert at position 717. The ectodomain structure appears as a 'folded-over' or 'tethered' conformation with an inverted 'V' shape [4], in which one leg comprises the L1-CR-L2 domains and the other FnIII-1, −2 and −3. However, the major drawback of the structure is that αCT is missing. Additionally, ID-α and ID-β are invisible [13]. More recent crystal structures include part of αCT, namely the segment 693–710, and, thus, provide more detailed insights into the structure of the ectodomain [11,14].

Structure of the transmembrane and juxtamembrane domains

The C-terminal of FnIII-3 is followed by the TM and JM domains, which are situated in the β-subunit and constitute approximately 80 amino acids (Fig. 1a), of which the TM domain (930–952) is predicted to represent 23 amino acids [15]. It is not understood how these two domains interact or what their relative orientation with respect to the holo-complex is. Recently, a fragment of residues 913–961 was expressed and purified in DPC micelles. NMR data showed that it adopted a well-defined α-helical structure from Leu935 to Tyr949, corresponding well to the predicted position of the TM helix but shortened by a kink introduced by residues Gly933 and Pro934 [16], as has also been predicted by molecular modeling [17]. Although this fragment was found to be mostly monomeric in the DPC micelles, cross-linking results provided evidence of dimer formation, implicating the cooperation of these domains in receptor activation, in line with earlier studies that showed that replacement of the IR TM helix sequence with the glycophorin helix sequence disrupted activation [15].

The JM domain (953–982) immediately following the TM helix has not yet been studied in its entirety. It is predicted to form a helix perpendicular to the membrane, although only the first ten residues were included in this simulation [17]. A crystal structure of the JM domain followed by the cytoplasmic domain showed no density for the residues preceding Ser974, after which it was helical. In the dimeric structure, the JM helical region interacts with α-helix C in the kinase domain of the other molecule and is proposed to function *cis*-autoinhibitory and activatory *in trans* [18].

Structure of the cytoplasmic domain

The CP domain of IR includes a TK domain (residues 980–1255 [7]) and an approximately 100-residue βCT domain [14] (Figs 1, 3 b,c). The TK domain comprises two lobes, in which the N-terminal lobe is composed of a twisted β-sheet with five antiparallel β-strands and one α-helix between the β3 and β4 sheets. The larger C-terminal lobe comprises eight α-helices and four β-strands. The catalytic cavity contains two short additional β-strands that traverse the cleft between the N- and C-terminal lobes [19]. Three Tyr phosphorylation sites, Tyr1158, Tyr1162 and Tyr1163 [20], are located in this catalytic cavity. Phosphorylation of Tyr1162 and/or Tyr1163, but not Tyr1158, has a critical role in the activation of TK [20]. There are also two Ser phosphorylation sites (Ser1275 and Ser1309) [21].

Insulin-binding sites in the IR ectodomain

Binding site 1: the L1-αCT harbor*

There are four insulin-binding sites in the dimeric receptor [4,22] (Fig. 2a). Binding site 1 (1′ in the other monomer) has a dissociation constant of [K_d] −6.4 nM and includes the β_2-sheet of the L1 domain (L1-β_2) and 16 residues of αCT* (*indicates that the amino acids arise from the paired monomer) [23–25]. This binding model has been tied to a 'cross-linking' mechanism of receptor activation and signal transduction [22,26,27]. However, the αCT* domain had not been visible in structures until recently, which draws into question the function of αCT* in receptor activation. The first structure that did include part of αCT* (residues 693–710) shed some light on its contribution to the interface [14]. Most recently, the direct interaction between insulin and binding site 1/1′ was presented by a truncated mutant including αCT* (residues 704–719), which highlighted two αCT* residues (His710 and Phe714) to be critical in the formation of the Insulin:$IR_{(L1\text{-}\alpha CT^*)}$ complex [10] (Fig. 2b,c). Unfortunately, no direct structural information, even in the most resolved structure [11], for residues 656–692 (part of ID-α) and 716–753 (including the end of αCT* and ID-β*) was provided, leaving the question open as to whether these domains also contribute to insulin binding. Based on the structural information available to date, it is clear that there are two components to the interaction of insulin with binding site 1/1′.

Formation of the L1-αCT* harbor

Along with IR dimer formation, a 'harbor' comprising αCT* and L1-$\beta_2\beta_3$ sheets is initiated (Fig. 2b) as follows: (i) residues Phe701 and Phe705 of αCT* are encompassed by residues Leu62, Phe64, Phe88, Phe89, Tyr91, Val94, Phe96, and Arg118 of the L1 domain; (ii) residue Tyr708 is packed nearly parallel to the central β-sheet plane of the L1 domain via interaction with residues Arg14, Gln34, Leu36, and Phe88; (iii) the spatially adjacent residue pair Glu698/Arg702 engages with the residue pair Arg118/Glu120, respectively, in a charge-compensation cluster. The side chains of Lys703/Asp707, which are close in space, contribute to charge compensation [4]; (iv) the side-chains of Leu709, Leu37, and Phe64 interact with each other; and (v) the hydrophobic face of αCT*, comprising residues Phe705, Tyr708, Leu709, Val712, and Val713, makes contact with a nonpolar groove on L1-β2 formed by residues Leu36, Leu37, Leu62, Phe64, Phe88, Phe89, Val94, and Phe96 [10,14,28].

Insulin engagement with the L1-αCT* harbor (Fig. 2c)

Previous work supported the conclusion that insulin binding to its primary site 1/1′ can be regarded as insulin docking to the L1-αCT* harbor through the following features: (i) His710 of αCT* inserts itself into a pocket formed by invariant insulin residues ValA3, GlyB8, SerB9, and ValB12 [26]; (ii) Phe714 occupies a hydrophobic crevice formed by invariant insulin residues GlyA1, IleA2, TyrA19, LeuB11, ValB12, and LeuB15; (iii) Asn711 is directed towards GlyA1, ValA3, and GluA4; and (iv) ValB12 is positioned between Phe39, Phe64, and Arg65, whereas TyrB16 adjoins Phe39 [10]. In

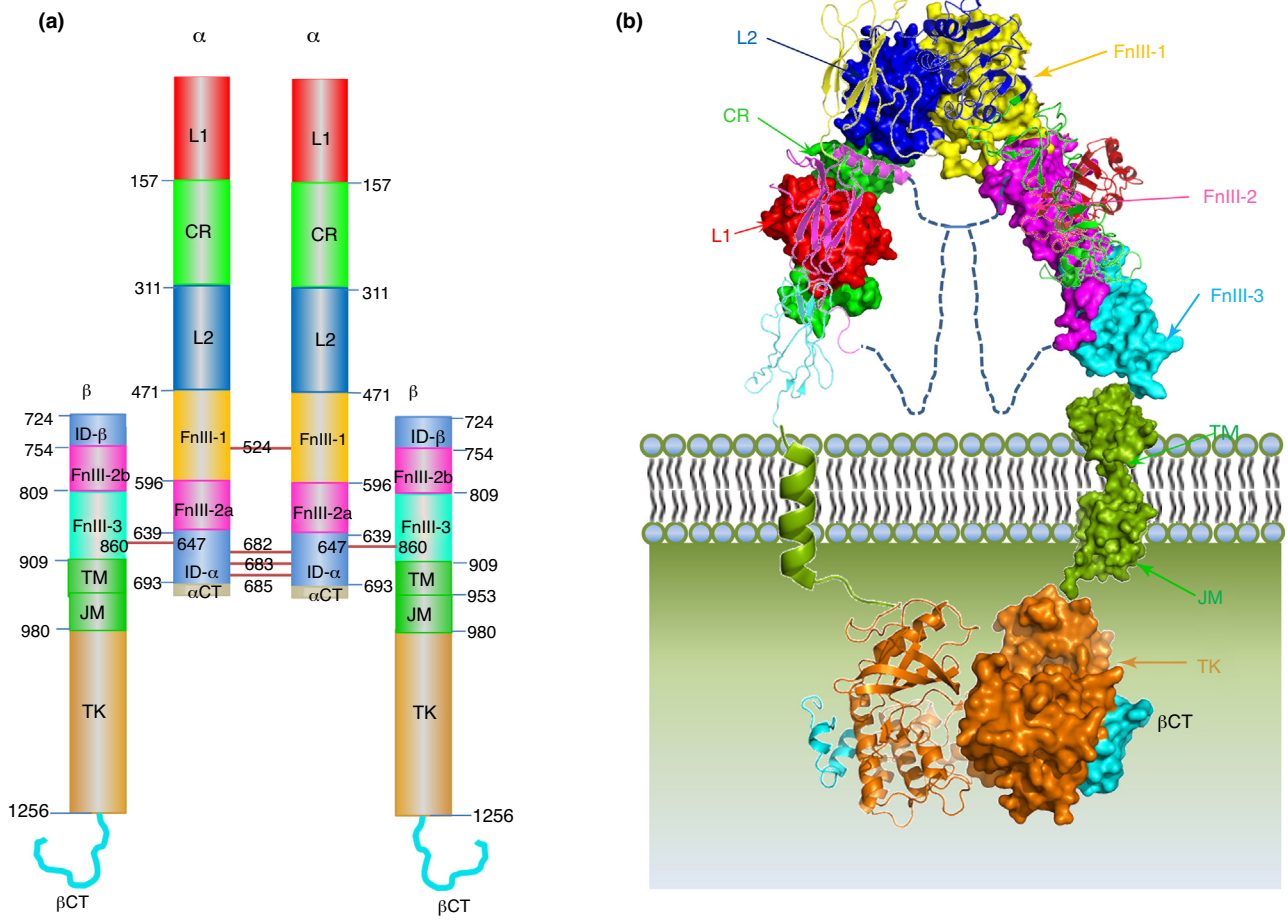

(c) Domain architectures of resolved IR structures	PDB IDs
L1 CR L2 FnIII-1 FnIII-2a ID-α αCT ID-β FnIII-2b FnIII-3 TM JM TK βCT	Composition of full-length IR (no structure)
	4ZXB [11], 3LOH [14]
	2DTG [13,78]
	3W14 [10]
	3W11, 3W12, 3W13 [10], 4OGA [29]
	2HR7 [23]
	2MFR [16]
	1IRK [9], 1IR3 [32], 1GAG [79], 1I44 [80], 1P14 [81], 2AUH [82], 2B4S [83], 3BU3, 3BU5, 3BU6 [84], 2Z8C [85], 4XLV [18]

Drug Discovery Today

FIGURE 1

Overview of insulin receptor (IR) domain architecture and currently structurally resolved components in the Protein Data Bank (PDB) database. **(a)** Domain organization schematic diagram for the full-length IR dimer. Residue numbering is obtained after removal of the signal peptide (27 residues). β-domain numbering follows IR-B. For a conversion of residue numbers from PDB structures to sequence positions see www.rcsb.org/pdb/protein/P06213. **(b)** Cartoon representation of the IR dimer structure. One receptor monomer is represented in secondary structure form, whereas the other monomer is as a surface

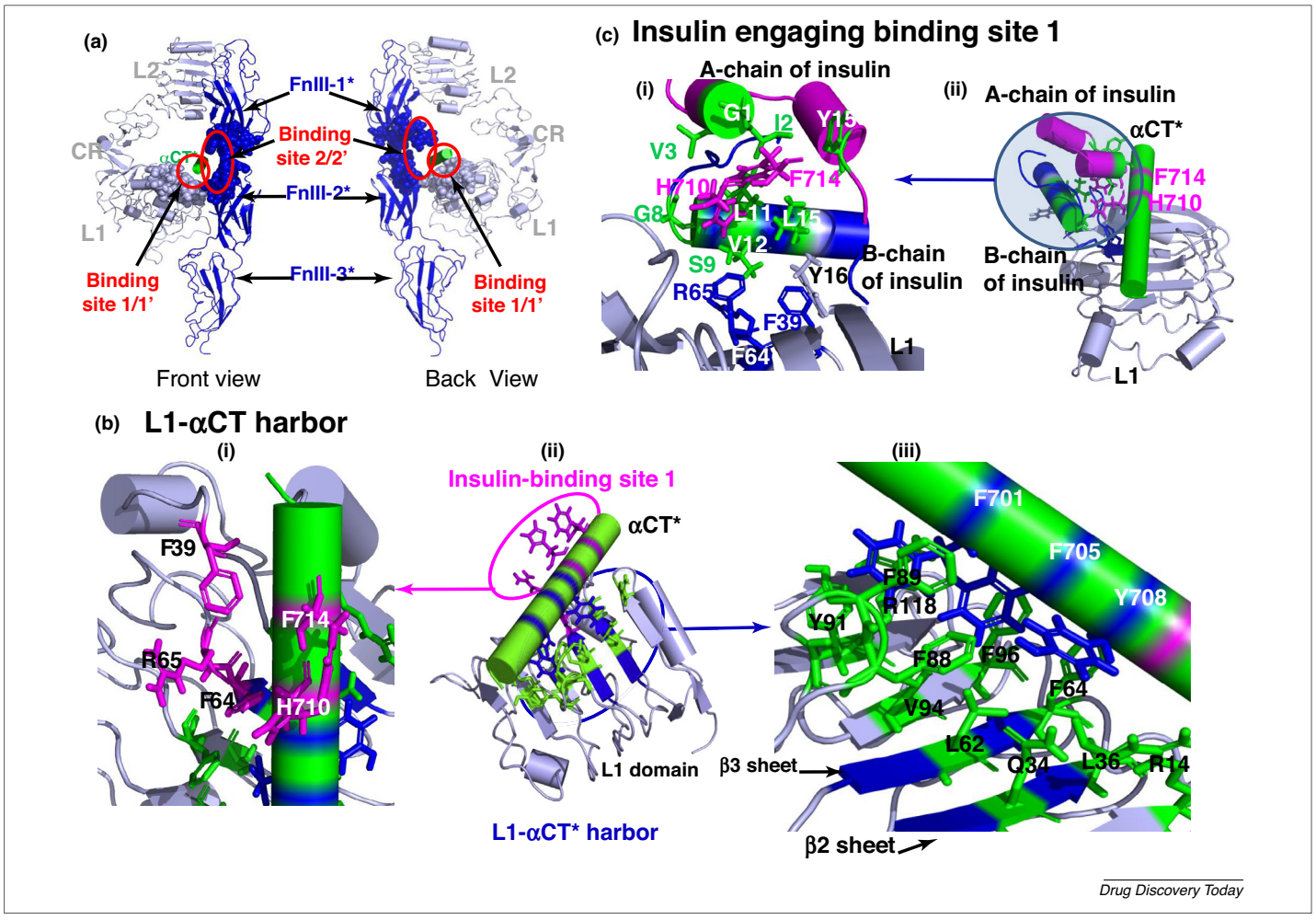

FIGURE 2

Structural insight into insulin receptor (IR) binding sites. **(a)** Overall views of binding sites 1 and 2 from the front and back views, respectively. L1, CR, and L2 domains from the first monomer are in gray, whereas fibronectin type III (FnIII)-1*, FnIII-2*, and FnIII-3* domains from the second monomer are in blue with an '*', and αCT* is shown in green. Binding site 1 comprises L1 and αCT* of FnIII-2* from the paired monomer. Binding site 2 comprises FnIII-1* and FnIII-2* from the second monomer. **(b)** Structural insight into binding site 1 with a detailed view of the αCT*-L1 complex (ii). The αCT* is in green, with critical residues Phe701, Phe705 and Tyr708, which interact with the L1 domain in blue. The critical residues from the L1 domain interacting with αCT* are colored in green (iii), and the interface of αCT*:L1 complex to insulin. The critical residues His710 and Phe714 from αCT*, and residues Phe39, Phe64 and Arg65 from the L1 domain are highlighted in pink (i). **(c)** Insulin binding model of receptor binding site 1. (i) View of the overall binding model. The A- and B-chains of insulin are in pink and blue, respectively, whereas αCT* is in green. The L1 domain is in gray. The two critical residues (His710 and Phe714) of αCT* that interact with insulin are in pink and the residues of insulin that interact with αCT* segment are in green. The residues of the L1 domain that interact with the B-chain of insulin are in blue. (ii) A detailed view of interactions between insulin and binding site 1 of the IR.

this mode, the insulin B-helix (CysB7-GluB21) engages the C-terminal end of the L1-β2 strands, whereas no interaction occurs between the A-chain and the L1 domain. Recently, it was discovered that there is a drastic relocation of αCT* upon insulin binding [28]. The relocation of αCT* containing residues 697–719 [10] upon insulin binding was explicitly observed in comparison with a shorter αCT* with residues 693–710 [14]. Previous biochemical evidence supports the conclusion that the C-terminus of the insulin β-chain, including residues GlyB23, PheB24, PheB25, and TyrB26 [7], has important roles in interacting with either αCT* or the L1 surface [10]. Most recently, it was demonstrated that the C-terminal B-chain segment was crucial to the interaction by undergoing concerted hinge-like rotation at its GlyB20–GlyB23 β-turn, coupling reorientation of the PheB24 residue to a 60° rotation of the PheB25–ProB28 β-strand away from the hormone core to lie antiparallel to the L1-αCT* harbor [29].

Binding site 2: junction of the C-terminal of FnIII-1 and the N-terminal of FnIII-2**

In contrast to binding site 1, which has been extensively investigated and experimentally documented, little is known about how insulin interacts with binding site 2. It has a [K_d] of −400 nM and involves no residues of the first monomer but rather loops located

representation. The colors for each domain correspond to (a). **(c)** Resolved IR components deposited so far in the PDB database. *αCT was only partially resolved in the structure. [Note that * indicates that the amino acids arise from the paired monomer].

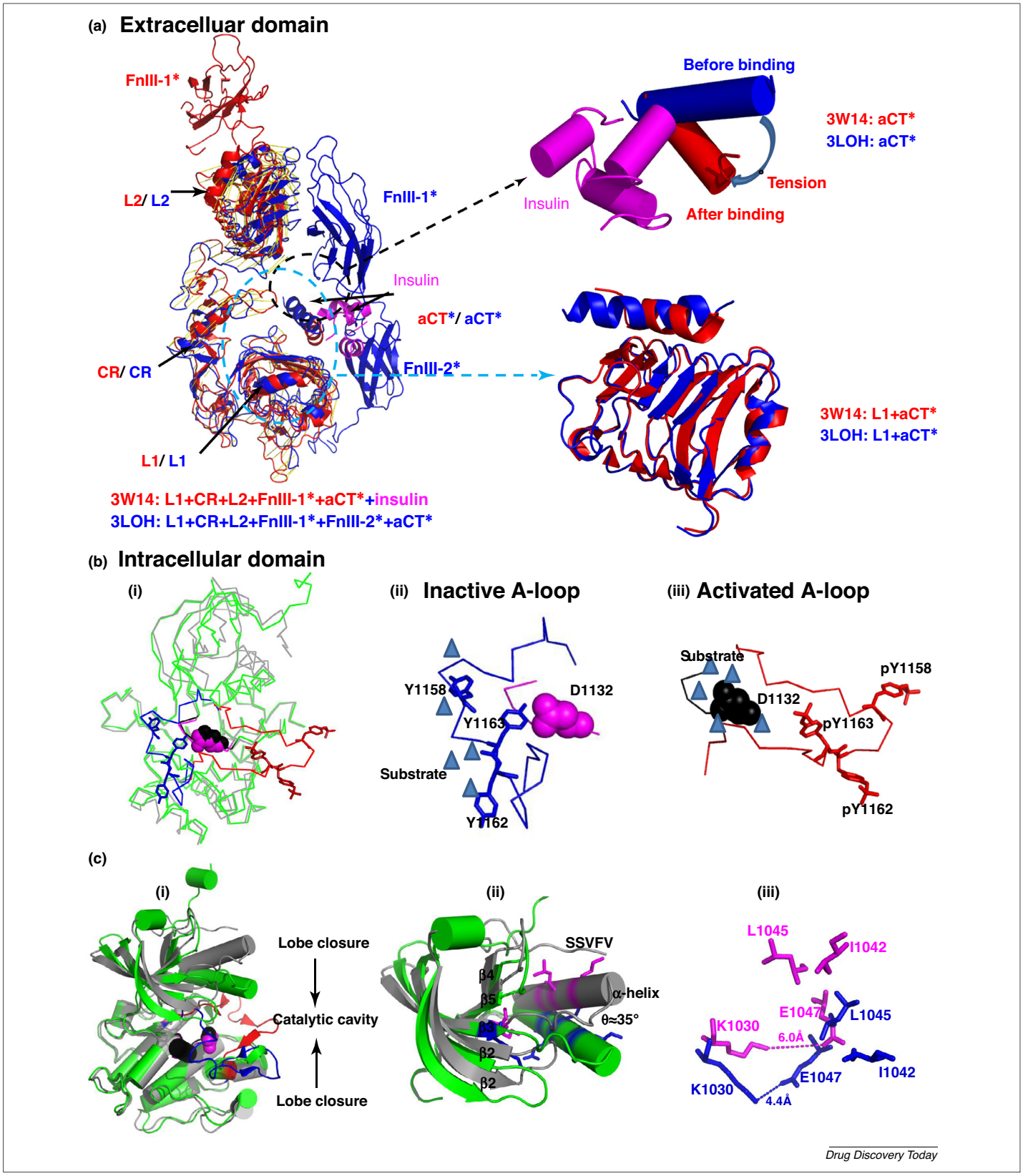

FIGURE 3

Conformational changes that result in insulin receptor (IR) activation (extracellular and intracellular). **(a)** Conformation comparison between 3LOH (without insulin) and 3W14 (with insulin). Note the difference in complexes L1 + αCT* and relocation angle of αCT* from entries 3LOH and 3W14. **(b)** Alignment of tyrosine kinase (TK) domains from 1IRK (inactive) and IRK (active), which are represented as Cα-traces. The backbones of 1IRK/IRK3 are in gray/green, with the A-loops colored blue/red and catalytic residues colored pink/black, respectively (i). Conformation of the A-loop (blue) and catalytic loop (pink) in 1IRK, with residues Tyr1158, Tyr1162, and Tyr1163 shown as sticks and Asp1132 shown as spheres (ii). Conformation of the A-loop (red) and catalytic loop (black) in IRK3, with residues Tyr1158, Tyr1162, and Tyr1163 shown as sticks and Asp1132 shown as spheres. The significant difference of these two conformations is IRK3

in the FnIII-1* and FnIII-2* domains from the paired monomer [4,13] on the opposite side of binding site 1. Specifically, residues Lys484, Leu552, and Asp591 of FnIII-1* and Ile602, Lys616, Asp620, and Pro621 of FnIII-2* have been implicated in binding [30]. Thus, the structure of the IR dimer indicates that ligand-binding site 2 is located opposite to the L1 face. This implies that, when insulin docks to site 1 (the L1-αCT* harbor, see above), the opposite side of the hormone will be facing this site [6,23]. Bioinformatics analysis of the IR family showed that residues located at the FnIII-1*–FnIII-2* junction, including Lys557 and Pro558 in the EF loop of FnIII-1*; Ser596, Val597, Pro598, Leu599, Asp600, and Pro601 at the start of FnIII-2*; Lys614, Trp615, and Lys616 in the B-strand of FnIII-2*; and Pro617, Pro618, and Pro621 in the BC loop of FnIII-2*, are conserved, which supports the hypothesis that these residues contribute to site 2 [31]. Inspection of FnII-1* and FnIII-2* regions and determination of solvent accessibilities suggested that the following residues could be involved in interaction with the hormone: Ser418 at the bottom of the A strand; Phe482 and Asp483 in the AB loop; Lys484 and Leu486 at the bottom of the B strand; Leu552 and Arg554 at the bottom of the E strand; Lys557 and Leu558 in the EF loop; Asp591 in the G strand; Thr593, Asn594, Pro595, Ser596, Val597, Leu599, Asp600, Pro601, and Ile602 in the intradomain linker; and Lys616, Pro617, Pro618, Ser619, Asp620, and Pro621 in the FnIII-2* domain [30]. Insulin binding to holoreceptors carrying Ala replacements at positions Lys484, Leu552, Asp591, Ile602, Lys616, Asp620,and Pro621 from binding site 2 showed two–fivefold increases in $IC_{50,}$ implying roles for these residues in binding [30]. To gain further insight into this interaction utilizing the structural information available to date, docking experiments were performed with the 3LOH structure (Ye et al., unpublished data, 2017) to study those residues that are predicted to be in direct contact with IR based on the most recently published crystal structures. A side-by-side comparison with the more recent 4ZXB structure revealed differences in predicted site 2 residues for the CC' loop, which is now largely missing. Therefore, those five amino acids that resulted only from 3LOH analysis in the above lists of residues were omitted in favor of those supported by both structures. Our experiments indicated that insulin residues SerA12, LeuA13, GluA17, HisB10, GluB13, and LeuB17 are predicted to be crucial for the interaction of insulin with binding site 2 of IR. These predictions are consistent with previous conclusions that these residues contribute to the second binding surface.

Conformational changes upon complex formation

Conformational changes in the IR ectodomain

The ectodomain structure of truncated L1-CR-L2-FnIII-1* containing αCT* (PDB: 3W14) in complex with insulin provided insight into the conformational change of the IR ectodomain in comparison to that of IR in complex with four Fab molecules [Protein Data Bank (PDB): 3LOH, recently replaced by the higher resolution 4ZXB structure, 3.3 Å in comparison to 3.8 Å, which also contains several reassignments and missing residues [11]] (Fig. 3a). Although one cannot rule out that αCT* was directly linked to FnIII-1* rather than to FnIII-2* in the structure of 3W14 and is a major contributor to the conformational change, the differences observed between 3W14 and 3LOH/4ZXB are likely a result of receptor activation. In particular, the relocation of αCT* upon insulin binding is a striking difference, as well as the L1 domain conformation change. Computational and docking experiments indicated that a slight opening of FnIII-1* and FnIII-2* is necessary to facilitate insulin entering into binding site 2 after its engagement with binding site 1, suggesting that such an opening is also part of the binding mechanism (Ye et al., unpublished data, 2017). Without further experimental validation, the precise nature and sequence of αCT* relocation, insulin engagement with sites 1 and 2, and conformational change of FnIII-1* and FnIII-2* remain unclear.

Conformational changes in the intracellular kinase domain

In the basal, inactive form of TK, the A-loop (residues 1149–1170) occupies the inactive TK enzyme gate within the catalytic cleft, effectively preventing substrates from approaching the catalytic center. The kinase-conserved ^{1150}DFG motif at the beginning of the A-loop also occupies the ATP binding site. Phosphorylation of Tyr1158, Tyr1162, and Tyr1163 results in a dramatic conformational change of the A-loop (Fig. 3bi) with displacement distances of approximately 31, approximately 23, and approximately 17 Å for these three Tyr residues before and after phosphorylation, respectively. This leads to the release of the A-loop (Fig. 3biii), making the binding sites for ATP and protein substrate accessible [32]. The tri-phosphorylated A-loop is stabilized by formation of hydrogen bonds of phospho-Tyr1162 and phospho-Tyr1163 with Arg1164 and Arg1155, respectively. Phospho-Tyr1158 does not significantly contribute to the stabilization of the active A-loop and is the least ordered among the phospho-Tyr residues. In the active A-loop, β10 is now paired with β12 while leaving its original partner β11 alone, which in turn allows β11 to interact with substrates [32]. The conformational change of the A-loop upon phosphorylation causes a reorientation of the N- and C-termini of the TK domain, which facilitates ATP binding. Both the N- and C-termini move toward the catalytic cavity (Fig. 3ci), forming a more compact and stable conformation. Relative to the C-terminal lobe, the N-terminal lobe experiences an overall rotation of −20° which comprises a twisted β-sheet of five antiparallel β-strands (β1-β5) and one α-helix. In particular, the most dramatic rotation is observed in the α-helix with $\theta \approx 35°$ (Fig. 3cii) [32]. The movement of this α-helix places the protein kinase-conserved residues Glu1047–Lys1030 into the ATP binding site by shortening the distance from 6.0 to 4.4 Å (Fig. 3ciii).

Concluding remarks, open questions, IR-triggering model, and drug development

How is αCT* relocation initiated? It has been proposed that the interaction between residue Asp707 of αCT* and residue GluA4 of

exposing the catalytic center to substrates (iii). **(c)** Alignment of TK domains from 1IRK and IRK3 represented in cylindrical cartoon format for outlining lobe closure of the N and C termini of the TK domain (i), and alignment of the β-sheets in the N-terminal lobes of 1IRK and IRK3 (ii). Conformation comparison of the ATP-binding site for 1IRK and IRK3 (iii). Inactive 1IRK residues are in pink, whereas IRK3 residues are in blue. Triangles represent substrates. The catalytic residue Asp1132 is shown in pink and black without and with substrate binding, respectively.

insulin triggers the conformational changes in the IR [28]. In support of this hypothesis, IR phosphorylation is nearly abolished in substitution mutant Asp707Ala [28]. However, it remains unclear how exactly this contact is formed, in particular how insulin approaches the receptor. It is clear that αCT* relocation enables access to binding sites 1 and 2, which enables insulin to enter more deeply into the binding cavity. If so, peptide mimetics of the αCT* segment could be potential inhibitors to decrease or block receptor activation. To our knowledge, no inhibitors mimicking αCT* have been reported so far and the function of αCT* proposed here could provide a new opportunity to develop such drugs.

Although the ectodomain structure of IR comprising L1, CR, L2, FnIII-1*, and αCT* in complex with insulin provided a detailed view of binding site 1 [10], the missing domains of FnIII-2* and FnIII-3* in the current structures resulted in an incomplete conformation depiction of the ectodomain. By comparing the ectodomains of 3W14 and 3LOH in Fig. 4a and b , one can see that FnIII-2a* and FnIII-2b* partially overlap, and the N terminus of FnIII-2a* is inserted into the FnIII-3* domain. A disulfide bond (Cys647–Cys860) between FnIII-2a* and FnIII-3* is proposed to serve as 'signaling bridge' to deliver the signal from the binding cavity upon insulin binding to FnIII-3* when αCT* is repositioned. Rotation of the FnIII-1* and FnIII-2* domains appears to be necessary to fully engage the structure with insulin and to transmit the binding signal into the CP domain [31]. A prerequisite of rotating FnIII-1* and FnIII-2* for full insulin engagement was also suggested by the observation that insulin (PBD ID: 1A7F; mutated at positions TyrB16, PheB24, and ThrB30) cannot be docked to the IR dimer structure (PBD: 3LOH) without modification. In the current structure, there is steric hindrance by these domains, preventing insulin entering binding site 2. Thus, a larger relative angle between the FnIII-1* and FnIII2* domains is necessary as insulin approaches the binding cavity.

It is believed that most TKs act as dimers [18,33,34]. While ligand-induced dimerization is a popular concept in receptor activation mechanisms [35–39], evidence also suggests that many receptors already perform as dimers before ligand engagement [40–43]. In particular, the two monomers in IR are already covalently linked by disulfide bonds, as shown in Fig. 1a [44], which suggests that IR does not fit the ligand-induced dimerization model. This highlights the need to explain what conformational changes occur in the dimer upon ligand binding to understand how the extracellular signal crosses the membrane as part of receptor activation. To begin filling this gap, a series of computational simulation and docking experiments were performed (Ye et al., unpublished data, 2017). As described above, insulin could only dock to the opposite face of the L1-αCT* harbor when the inactive L1-αCT* component from the 3LOH/4ZXB structure was used for computational docking. Insulin can easily dock to an activated L1-*αCT harbor when *αCT has been moved away but cannot completely enter into the binding cavity involving both binding sites 1 and 2. This suggests that, in addition to *αCT movement, an opening of FnIII-1* and FnIII-2* domains is necessary to form a bigger binding cavity. The αCT* helix could serve as a lever to help FnIII-1* and FnIII-2* movements. Given that the receptor functions as a dimer, herein, we propose a novel triggering model, termed the 'bow-arrow model', because the receptor motion upon insulin binding can be visualized analogous to the process of relaxation of tension in the bow at the moment an arrow leaves the bow (Fig. 4d). [Note there is no physical equivalent of an 'arrow' in the IR system.] Relocation of αCT* is triggered upon insulin approaching the receptor, and the tension of the bent IR ectodomain conformation is released and momentum delivered to FnIII-2a* and FnIII-3* through ID-α* and the Cys647–Cys860 disulfide bond. This provides the means for rearrangement of the FnIII-1* and FnIII-2* domains to create a bigger cavity to properly allow insulin binding. Subsequently, FnIII-3* will receive the rearranged conformational signal from binding site 2′ because insulin is now completely accommodated into the binding cavity. The proximity of FnIII-3* to the TM domain makes it likely that the TM domain is affected and the signal pulse can now be transmitted across the membrane to the TK domain.

The new model also provides a new framework to discuss the functional properties of the IR. For example, negative cooperativity is a hallmark of the IR [45]. We propose that, after relaxation of the tension in the empty receptor, the resulting sluggish conformation prohibits insulin contact to trigger displacement of αCT coupled to conformational change. The model also predicts that low-affinity site 2 is already exposed and high-affinity site 1 altered so that the second insulin molecule binds with overall lower affinity and dissociates faster. Another interesting question is the mechanism of action of those disease-causing mutations in IR that are associated with altered insulin binding [46]. According to the insulin-bound crystal structure 3W15, Asn15 (when mutated to Lys with a fivefold decrease in insulin affinity) is in direct contact with insulin site 1, the L1-αCT harbor, and interferes with Arg14 packing to Tyr708 (Fig. 2b). More difficult is the interpretation of Lys460Glu, which increases insulin affinity, yet causes insulin resistance. Inspection of the structure shows that Lys460 is not in direct contact with insulin. Rather, it is located near the L2–FnIII-1* interface, which contributes to the scaffold that creates site 2. Thus, it is tempting to speculate that the previously proposed allosteric effects of this mutation are mediated by disruption of the bow-arrow mechanism through impairment of the proposed FnIII-1*/FnIII-2* opening required for site 2 engagement. Finally, the central role of the αCT segment for insulin binding at both sites −1 and −2, and the role that its relative position and flexibility is proposed to have in activation (Fig. 4d), emphasize why the 12-amino acid insert found in IR-B, adjacent to the Phe714 side of αCT in contact with insulin (Fig. 2b), would be expected to modulate the affinity, specificity, and activity of the receptor, a fact that was recently used in IR-B preferential targeting by IR isoforms [47].

Although it is not necessary to completely understand the conformational changes and signal transduction upon insulin binding for drug development, mechanistic knowledge of the basis of hormone binding can provide detailed insight for the design of receptor agonists or antagonists [7]. Existing molecules are insulin peptide analogs (e.g., lispro, aspart, glulisine, glargine, and detemir [48]), dimerized small ligands that mimic the natural ligand, allosteric activators, small ligands that stabilize a receptor–dimer interface, direct activators of the TK domain of IR, and direct activators of the signal-transduction pathways. Numerous drugs are known to act on the IR signaling cascade via different mechanisms: Merck's L7 [49,50] and its analog

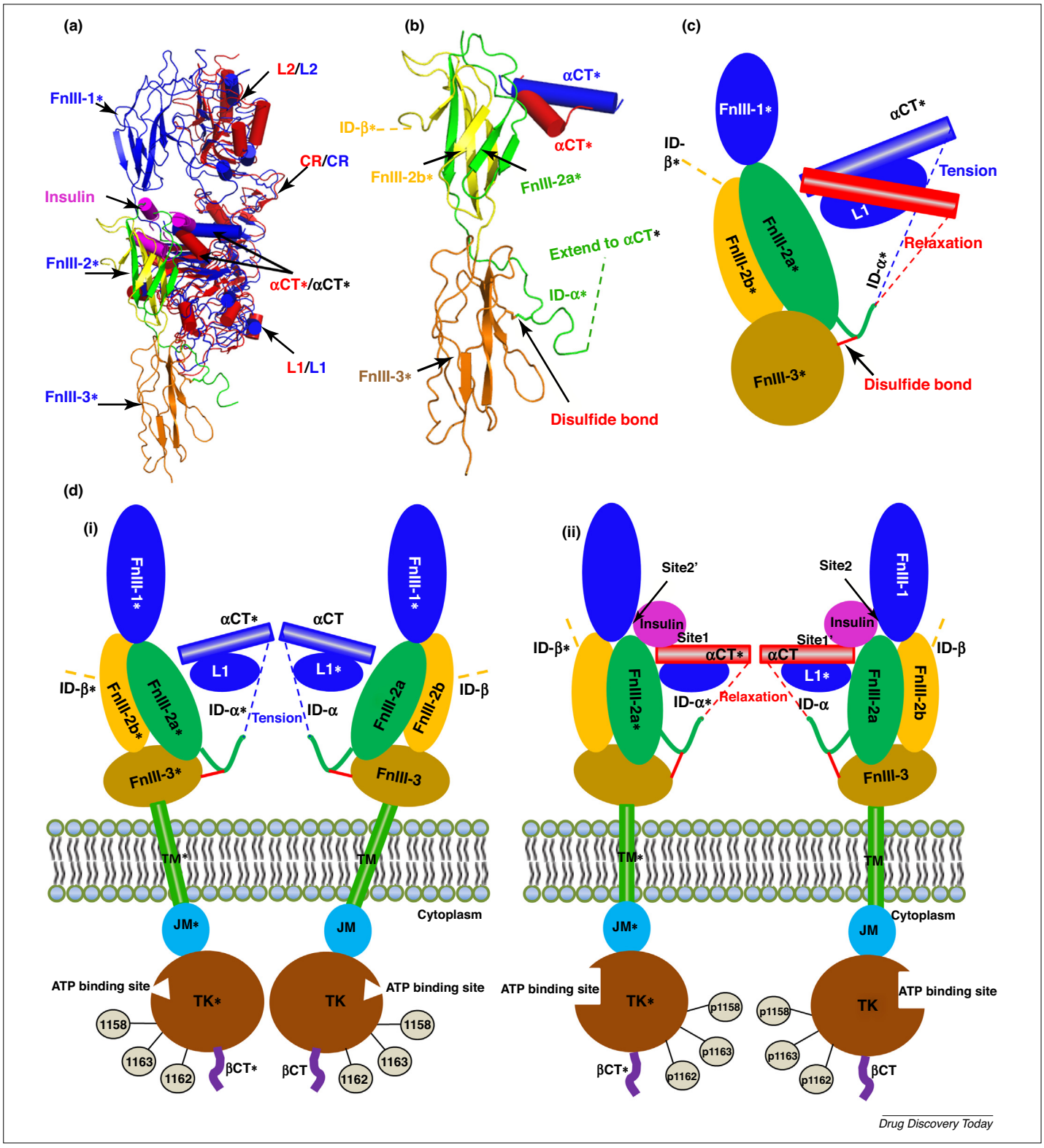

FIGURE 4

Proposed conformational change of domains fibronectin type III (FnIII)-1*, FnIII-2*, FnIII-3*, and peptide αCT* and insulin receptor (IR) activation model. **(a)** Alignment of 3W14 (red) and 3LOH (blue), in which FnIII-2* is in yellow or green, FnIII-3* is in dark yellow and insulin is in pink. **(b)** Magnification of FnIII-2* and FnIII-3* with more detailed structural information. **(c)** Schematic diagram of proposed conformational changes within FnIII-2* and FnIII-3* domains of IR upon insulin binding. **(d)** A proposed tyrosine kinase (TK) activity-triggering model, termed here the 'bow-arrow model', based on the conformational change of IR when going from an inactive (i) to active (ii) state (for details, see the main text).

TABLE 1

Summary of activators and inhibitors of insulin receptor

Substance	Mechanism of action	Effect	Refs
S597	Binding to, and phosphorylation of, IR	Stimulation of lipogenesis in mouse adipocytes *in vitro*	[66]
CG7 (ursolic acid)	IR activator by enhancing IR β-subunit autophosphorylation and subsequent downstream signaling	Stimulation of glucose uptake in cells *in vitro* and *in vivo*	[67,68]
XMEtA	Binding to IR, acting allosterically	Glucose uptake enhanced at subnanomolar concentrations by both insulin and XMetA *in vitro*	[69]
4548-G05	Activator of IR	Stimulation of glucose uptake in cells *in vitro*, decrease in the levels of blood glucose *in vivo*	[70]
TLK19780	IR activators by increasing β-subunit TK activity	Enhancement of increased insulin sensitivity and maximal responsiveness to insulin *in vitro*	[57]
TLK16998	IR sensitizers by enhancing IR autophosphorylation	Enhancement of increased insulin sensitivity, stimulation of glucose uptake in cells *in vitro*, decrease in levels of blood glucose *in vivo*	[56,71]
TLK 19781 (Compound 1)	Binding to IR intracellular region close to kinase domain and multiple Tyr phosphorylation sites	Increase in glucose sensitivity *in vivo*	[72]
6Cl-TGQ	Phosphorylation of IR	Stimulation of glucose uptake in cell for a long time *in vitro*, decrease in levels of blood glucose and insulin, improvement of glucose tolerance *in vivo*	[73]
L-783,281 (dimetilasterrihinon, DMAQ-B1); 2,5-dihydroxy-6- (1-methyl indol-3-yl)-3-phenyl-1,4-benzoquinone (Compound 2)	IR activators by increasing β-subunit TK activity directly through autophosphorylation	Decrease in levels of blood glucose and hyperinsulinemia *in vivo*	[55,74]
Thymolphthalein	Binding to IR, auto- and substrate phosphorylation of IR	Potentiates lipogenesis in adipocytes in presence of submaximal concentrations of insulin *in vivo*	[75]
Subetta	Modulate effects on β-subunit of IR via modification of its conformation	Increase in β-subunit phosphorylation of IR with and without insulin *in vitro*, stimulates insulin-dependent glucose uptake *in vitro*, stimulation of adiponectin secretion *in vitro*, decreases blood glucose level and improves glucose tolerance *in vivo*	[60,63,64,76,77]

Compound 2 [51,52], 6Cl-TGQ [53], DMAQ-B1 [54], and 2,5-dihydroxy-6-(1-methylindol-3-yl)-3-phenyl-1,4-benzoquinone [55] are IR activators that increase β-subunit TK activity directly through autophosphorylation even in the absence of insulin. Telik's TLK16998 [49,56] and TLK19780 [57] are IR sensitizers that enhance IR autophosphorylation instead of directly activating IR autophosphorylation in the presence of insulin. Morin [58] is a noncompetitive inhibitor of PTP1B. Docking simulations show that it binds to the noncatalytic phospho-Tyr site B and not to the substrate site (site A) of PTP1B [58]. The interactions with site B are via the formation of hydrogen bonds and hydrophobic interactions of the Morin ring. A novel class of arylalkylamine vanadium salts [59] are activators of the intracellular insulin-signaling pathway downstream independently of IR activation. MATERIA MEDICA HOLDING's Subetta [60], a novel complex drug containing released-active forms of antibodies to the β-subunit of the IR [61] and antibodies to endothelial nitric oxide synthase, exerts a modulating effect on the β-subunit of the IR via modification of its conformation [62]. This results in an increase in the phosphorylation of the β-subunit [63] and stimulation of insulin-induced glucose uptake [64]. Most of the above mentioned compounds show antidiabetic effects in animal models, supporting the *in vitro* data describing their action on the IR (Table 1). Interestingly, a synthetic peptide, 'IR-TM', corresponding to the TM domain, activates the receptor, supporting the hypothesis that insulin-dependent ectodomain activation can be bypassed by direct interaction with and, thus, potential disruption of a dimerized TM domain [65]. Thus, all of the domains of the IR have the potential to be drug targets.

Here, we have provided a more comprehensive view of the structure and dynamics of the insulin–IR interaction by summarizing published data and hypotheses deduced from alignment and computational simulation. We hope that the insight gained not only enhances our understanding of the mechanism of TK activation, but might also benefit targeted drug development to tackle diabetes mellitus.

References not cited elsewhere in the text: [78–85].

Acknowledgments

Funding was provided by Materia Medica Holding, Russian Federation.

References

1 Seino, S. *et al.* (1989) Structure of the human insulin receptor gene and characterization of its promoter. *Proc. Natl. Acad. Sci. U. S. A.* 86, 114–118
2 Schenker, E. and Kohanski, R.A. (1991) The native $\alpha_2\beta_2$ tetramer is the only subunit structure of the insulin receptor in intact cells and purified receptor preparations. *Arch. Biochem. Biophys.* 290, 79–85
3 Massague, J. *et al.* (1980) Electrophoretic resolution of three major insulin receptor structures with unique subunit stoichiometries. *Proc. Natl. Acad. Sci. U. S. A.* 77, 7137–7141
4 Ward, C.W. and Lawrence, M.C. (2012) Similar but different: ligand-induced activation of the insulin and epidermal growth factor receptor families. *Curr. Opin. Struct. Biol.* 22, 360–366
5 Kavran, J.M. *et al.* (2014) How IGF-1 activates its receptor. *elife* 3, e03772
6 Lawrence, M.C. *et al.* (2007) Insulin receptor structure and its implications for the IGF-1 receptor. *Curr. Opin. Struct. Biol.* 17, 699–705
7 De Meyts, P. and Whittaker, J. (2002) Structural biology of insulin and IGF1 receptors: implications for drug design. *Nat. Rev. Drug Discov.* 1, 769–783
8 Kasuga, M. *et al.* (1982) Insulin stimulation of phosphorylation of the beta subunit of the insulin receptor. Formation of both phosphoserine and phosphotyrosine. *J. Biol. Chem.* 257, 9891–9894
9 Hubbard, S.R. *et al.* (1994) Crystal structure of the tyrosine kinase domain of the human insulin receptor. *Nature* 372, 746–754
10 Menting, J.G. *et al.* (2013) How insulin engages its primary binding site on the insulin receptor. *Nature* 493, 241–245
11 Croll, T.I. *et al.* (2016) Higher-resolution structure of the human insulin receptor ectodomain: multi-modal inclusion of the insert domain. *Structure* 24, 469–476
12 Lukman, S. *et al.* (2015) Harnessing structural data of insulin and insulin receptor for therapeutic designs. *J. Endocrinol. Metab.* 5, 273–283
13 McKern, N.M. (2006) Structure of the insulin receptor ectodomain reveals a folded-over conformation. *Nature* 443, 218–221
14 Smith, B.J. (2010) Structural resolution of a tandem hormone-binding element in the insulin receptor and its implications for design of peptide agonists. *Proc. Natl. Acad. Sci. U. S. A.* 107, 6771–6776
15 Gardin, A. *et al.* (1999) Substitution of the insulin receptor transmembrane domain with that of glycophorin A inhibits insulin action. *FASEB J.* 13, 1347–1357
16 Li, Q. *et al.* (2014) Solution structure of the transmembrane domain of the insulin receptor in detergent micelles. *Biochim. Biophys. Acta* 1838, 1313–1321
17 Mohammadiarani, H. and Vashisth, H. (2016) All-atom structural models of the transmembrane domains of insulin and type 1 insulin-like growth factor receptors. *Front. Endocrinol.* 7, 68
18 Cabail, M.Z. *et al.* (2015) The insulin and IGF1 receptor kinase domains are functional dimers in the activated state. *Nat. Commun.* 6, 6406
19 Denley, A. *et al.* (2003) The insulin receptor isoform exon 11- (IR-A) in cancer and other diseases: a review. *Hormone Metab. Res.* 35, 778–785
20 Zhang, B. *et al.* (1991) The regulatory role of known tyrosine autophosphorylation sites of the insulin receptor kinase domain. An assessment by replacement with neutral and negatively charged amino acids. *J. Biol. Chem.* 266, 990–996
21 Tennagels, N. *et al.* (2001) Identification of Ser(1275) and Ser(1309) as autophosphorylation sites of the human insulin receptor in intact cells. *Biochem. Biophys. Res. Commun.* 282, 387–393
22 Ward, C.W. and Lawrence, M.C. (2009) Ligand-induced activation of the insulin receptor: a multi-step process involving structural changes in both the ligand and the receptor. *Bioessays* 31, 422–434
23 Lou, M. *et al.* (2006) The first three domains of the insulin receptor differ structurally from the insulin-like growth factor 1 receptor in the regions governing ligand specificity. *Proc. Natl. Acad. Sci. U. S. A.* 103, 12429–12434
24 Kurose, T. *et al.* (1994) Cross-linking of a B25 azidophenylalanine insulin derivative to the carboxyl-terminal region of the alpha-subunit of the insulin receptor. Identification of a new insulin-binding domain in the insulin receptor. *J. Biol. Chem.* 269, 29190–29197
25 Mynarcik, D.C. *et al.* (1997) Analog binding properties of insulin receptor mutants: Identification of amino acids interacting with the COOH terminus of the B-chain of the insulin molecule. *J. Biol. Chem.* 272, 2077–2081
26 De Meyts, P. *et al.* (2004) Structural biology of insulin and IGF-1 receptors. *Novartis Found. Symp.* 262, 160–171 discussion 171–166, 265–168
27 Kiselyov, V.V. *et al.* (2009) Harmonic oscillator model of the insulin and IGF1 receptors' allosteric binding and activation. *Mol. Syst. Biol.* 5, 243
28 Whittaker, J. *et al.* (2012) alpha-Helical element at the hormone-binding surface of the insulin receptor functions as a signaling element to activate its tyrosine kinase. *Proc. Natl. Acad. Sci. U. S. A.* 109, 11166–11171
29 Menting, J.G. *et al.* (2014) Protective hinge in insulin opens to enable its receptor engagement. *Proc. Natl. Acad. Sci. U. S. A.* 111, E3395–E3404
30 Whittaker, L. *et al.* (2008) High-affinity insulin binding: insulin interacts with two receptor ligand binding sites. *Biochemistry* 47, 12900–12909
31 Renteria, M.E. *et al.* (2008) A comparative structural bioinformatics analysis of the insulin receptor family ectodomain based on phylogenetic information. *PLoS One* 3, e3667
32 Hubbard, S.R. (1997) Crystal structure of the activated insulin receptor tyrosine kinase in complex with peptide substrate and ATP analog. *EMBO J.* 16, 5572–5581
33 Maruyama, I.N. (2014) Mechanisms of activation of receptor tyrosine kinases: monomers or dimers. *Cells* 3, 304–330
34 Endres, N.F. *et al.* (2014) Emerging concepts in the regulation of the EGF receptor and other receptor tyrosine kinases. *Trends Biochem. Sci.* 39, 437–446
35 Ullrich, A. and Schlessinger, J. (1990) Signal transduction by receptors with tyrosine kinase activity. *Cell* 61, 203–212
36 Lemmon, M.A. and Schlessinger, J. (2010) Cell signaling by receptor tyrosine kinases. *Cell* 141, 1117–1134
37 Liu, H. *et al.* (2007) Structural basis for stem cell factor-KIT signaling and activation of class III receptor tyrosine kinases. *EMBO J.* 26, 891–901
38 Leppanen, V.M. *et al.* (2010) Structural determinants of growth factor binding and specificity by VEGF receptor 2. *Proc. Natl. Acad. Sci. U. S. A.* 107, 2425–2430
39 Bublil, E.M. and Yarden, Y. (2007) The EGF receptor family: spearheading a merger of signaling and therapeutics. *Curr. Opin. Cell Biol.* 19, 124–134
40 Tao, R.H. and Maruyama, I.N. (2008) All EGF(ErbB) receptors have preformed homo- and heterodimeric structures in living cells. *J. Cell Sci.* 121, 3207–3217
41 Moriki, T. *et al.* (2001) Activation of preformed EGF receptor dimers by ligand-induced rotation of the transmembrane domain. *J. Mol. Biol.* 311, 1011–1026
42 Yu, X. *et al.* (2002) Ligand-independent dimer formation of epidermal growth factor receptor (EGFR) is a step separable from ligand-induced EGFR signaling. *Mol. Biol. Cell* 13, 2547–2557
43 Clayton, A.H. *et al.* (2005) Ligand-induced dimer-tetramer transition during the activation of the cell surface epidermal growth factor receptor-A multidimensional microscopy analysis. *J. Biol. Chem.* 280, 30392–30399
44 Ward, C.W. *et al.* (2007) The insulin and EGF receptor structures: new insights into ligand-induced receptor activation. *Trends Biochem. Sci.* 32, 129–137
45 de Meyts, P. *et al.* (1973) Insulin interactions with its receptors: experimental evidence for negative cooperativity. *Biochem. Biophys. Res. Commun.* 55, 154–161
46 Taylor, S. (1992) Lilly Lecture: molecular mechanisms of insulin resistance: lessons from patients with mutations in the insulin-receptor gene. *Diabetes* 41, 1473–1490
47 Vikova, J. *et al.* (2016) Rational steering of insulin binding specificity by intra-chain chemical crosslinking. *Sci. Rep.* 6, 19431
48 Varewijck, A.J. and Janssen, J.A. (2012) Insulin and its analogues and their affinities for the IGF1 receptor. *Endocr. Relat. Cancer* 19, F63–F75
49 Li, M. *et al.* (2001) Small molecule insulin receptor activators potentiate insulin action in insulin-resistant cells. *Diabetes* 50, 2323–2328
50 Zhang, B. *et al.* (1999) Discovery of a small molecule insulin mimetic with antidiabetic activity in mice. *Science* 284, 974–977
51 Qureshi, S.A. *et al.* (2000) Activation of insulin signal transduction pathway and anti-diabetic activity of small molecule insulin receptor activators. *J. Biol. Chem.* 275, 36590–36595
52 Ding, V.D. *et al.* (2002) Regulation of insulin signal transduction pathway by a small-molecule insulin receptor activator. *Biochem. J.* 367, 301–306
53 Cao, Y. *et al.* (2013) Orally efficacious novel small molecule 6-chloro-6-deoxy-1,2,3,4-tetra-O-galloyl-alpha-D-glucopyranose selectively and potently stimulates insulin receptor and alleviates diabetes. *J. Mol. Endocrinol.* 51, 15–26
54 Salituro, G.M. *et al.* (2001) Discovery of a small molecule insulin receptor activator. *Rec. Progr. Hormone Res.* 56, 107–126
55 Liu, K. *et al.* (2000) Discovery of a potent, highly selective, and orally efficacious small-molecule activator of the insulin receptor. *J. Med. Chem.* 43, 3487–3494
56 Manchem, V.P. *et al.* (2001) A novel small molecule that directly sensitizes the insulin receptor *in vitro* and *in vivo*. *Diabetes* 50, 824–830
57 Pender, C. *et al.* (2002) Regulation of insulin receptor function by a small molecule insulin receptor activator. *J. Biol. Chem.* 277, 43565–43571
58 Paoli, P. *et al.* (1830) The insulin-mimetic effect of Morin: a promising molecule in diabetes treatment. *Biochim. Biophys. Acta* 3102–3111
59 García-Vicente, S. *et al.* (2007) Oral insulin-mimetic compounds that act independently of insulin. *Diabetes* 56, 486–493
60 Bailbe, D. *et al.* (2013) The novel oral drug Subetta exerts an antidiabetic effect in the diabetic Goto-Kakizaki rat: comparison with rosiglitazone. *J. Diabetes Res.* 2013, 763125

61 Epstein, O.I. (2013) The phenomenon of release activity and the hypothesis of 'spatial' homeostasis. *Usp. Fiziol. Nauk* 44, 54–76

62 Epstein, O.I. (2012) Release-activity: a long way from phenomenon to new drugs. *Bull. Exp. Biol. Med.* 154, 54–58

63 Gorbunov, E.A. *et al.* (2015) Subetta increases phosphorylation of insulin receptor beta-subunit alone and in the presence of insulin. *Nutr. Diabetes* 5, e169

64 Gorbunov, E.A. *et al.* (2015) Subetta enhances sensitivity of human muscle cells to insulin. *Bull. Exp. Biol. Med.* 159, 463–465

65 Lee, J. *et al.* (2014) Insulin receptor activation with transmembrane domain ligands. *J. Biol. Chem.* 289, 19769–19777

66 Rajapaksha, H. and Forbes, B.E. (2015) Ligand-binding affinity at the insulin receptor isoform-A and subsequent IR-A tyrosine phosphorylation kinetics are important determinants of mitogenic biological outcomes. *Front. Endocrinol.* 6, 107

67 Jung, S.H. *et al.* (2007) Insulin-mimetic and insulin-sensitizing activities of a pentacyclic triterpenoid insulin receptor activator. *Biochem. J.* 403, 243–250

68 He, Y. *et al.* (2014) Ursolic acid increases glucose uptake through the PI3 K signaling pathway in adipocytes. *PLoS One* 9, e110711

69 Bedinger, D.H. *et al.* (2015) Differential pathway coupling of the activated insulin receptor drives signaling selectivity by XMetA, an allosteric partial agonist antibody. *J. Pharmacol. Exp. Ther.* 353, 35–43

70 Qiang, G. *et al.* (2014) Identification of a small molecular insulin receptor agonist with potent antidiabetes activity. *Diabetes* 63, 1394–1409

71 Altaf, Q.A. *et al.* (2015) Novel therapeutics for type 2 diabetes: insulin resistance. *Diabetes Obes. Metab.* 17, 319–334

72 Wu, M. *et al.* (2015) Potentiation of insulin-mediated glucose lowering without elevated hypoglycemia risk by a small molecule insulin receptor modulator. *PLoS One* 10, e0122012

73 Cao, Y. *et al.* (2014) Biological and biomedical functions of Penta-O-galloyl-D-glucose and its derivatives. *J. Nat. Med.* 68, 465–472

74 Tsai, H.J. and Chou, S.-Y. (2009) A novel hydroxyfuroic acid compound as an insulin receptor activator −structure and activity relationship of a prenylindole moiety to insulin receptor activation. *J. Biomed. Sci.* 16, 68

75 Schlein, M. *et al.* (2001) Properties of small molecules affecting insulin receptor function. *Biochemistry* 40, 13520–13528

76 Nicoll, J. *et al.* (2013) Subetta treatment increases adiponectin secretion by mature human adipocytes in vitro. *J. Endocrinol.* 925874

77 Kheyfets, I.A. *et al.* (2012) Study of hypoglycemic activity of Subetta and rosiglitazone on the model of streptozotocin-induced diabetes mellitus in rats. *Bull. Exp. Biol. Med.* 153, 54–56

78 Schaffer, L. *et al.* (2003) Assembly of high-affinity insulin receptor agonists and antagonists from peptide building blocks. *Proc. Natl. Acad. Sci. U. S. A.* 100, 4435–4439

79 Parang, K. *et al.* (2001) Mechanism-based design of a protein kinase inhibitor. *Nat. Struct. Biol.* 8, 37–41

80 Till, J.H. *et al.* (2001) Crystallographic and solution studies of an activation loop mutant of the insulin receptor tyrosine kinase: insights into kinase mechanism. *J. Biol. Chem.* 276, 10049–10055

81 Li, S. *et al.* (2003) Structural and biochemical evidence for an autoinhibitory role for tyrosine 984 in the juxtamembrane region of the insulin receptor. *J. Biol. Chem.* 278, 26007–26014

82 Depetris, R.S. *et al.* (2005) Structural basis for inhibition of the insulin receptor by the adaptor protein Grb14. *Mol. Cell.* 20, 325–333

83 Li, S. *et al.* (2005) Crystal structure of a complex between protein tyrosine phosphatase 1 B and the insulin receptor tyrosine kinase. *Structure* 13, 1643–1651

84 Wu, J. *et al.* (2008) Structural and biochemical characterization of the KRLB region in insulin receptor substrate-2. *Nat. Struct. Mol. Biol.* 15, 251–258

85 Katayama, N. *et al.* (2008) Identification of a key element for hydrogen-bonding patterns between protein kinases and their inhibitors. *Proteins* 73, 795–801